Surface Interactions in a Shear Field

Laura J. Dietsche, Morton M. Denn, and Alexis T. Bell
Dept. of Chemical Engineering, University of California at Berkeley,
and Center for Advanced Materials, Lawrence Berkeley Laboratory, Berkeley, CA 94720

The dynamics of chain exchange between flowing bulk melt and the channel wall were studied for oligomeric polyolefins using attenuated total reflectance Fourier transform infrared spectroscopy (ATR/FTIR). The dynamics are dominated by a surprisingly slow first-order process which depends on flow rate and materials of construction of the channel wall. The picture which seems to emerge is an entropically-driven flow-rate- (or stress-) dependent adsorption equilibrium which retards the exchange between the surface and bulk.

Introduction

The interaction between a fluid and a solid surface in shear flow is of fundamental importance in many areas of technology, including polymer processing. We are particularly interested in a polymer extrusion instability known as melt fracture, which is believed by some workers to be associated with a loss of adhesion at the polymer/metal interface ("slip"). The relevant literature is summarized in Denn (1992); a particularly provocative set of experiments by Ramamurthy (1986), in which replacement of a chrome-plated steel die by an alpha-brass die delayed or eliminated the onset of melt fracture in linear polyethylene, is strongly suggestive of a surface-induced mechanism. It is known that additives (antioxidants and "flow modifiers") can enhance or suppress the onset of melt fracture, and it is likely that they are active at the surface.

The current study was designed to obtain information about the dynamics of chain exchange between a sheared polymer melt and the solid bounding surface. We have designed a flow system in which the planar face of a hemicylindrical optical crystal forms one side of a channel, and we have used attenuated total reflectance (ATR) Fourier transform infrared spectroscopy (FTIR) to study the displacement of an oligomeric polyolefin at the surface by a similar molecule. Granick and coworkers (see Granick, 1992; Douglas et al., 1993; Johnson et al., 1993) have used ATR/FTIR to study the adsorption and desorption of polymer chains from solution, but this is the first study of exchange from the melt. The exchange rates were obtained as a function of flow rate for three different surfaces. While the system was designed for macromolecular melts, the experiments reported here were carried out on C-16 oligomers (*n*-hexadecane and 1-hexadecene) in order to operate near atmospheric pressure and room temperature. The system was selected to mimic the weak interactions between polyolefins and metal dies. The results indicate a surprising reduction in the mobility of the chains at the surface, with interaction effects that are strongly dependent on the nature of the surface.

Correspondence concerning this article should be addressed to M. M. Denn.
Present address of L. J. Dietsche: Dow Chemical, Midland, MI 48674.

Experimental System

The ATR flowcell, shown in Figures 1 and 2, was built to our specifications by Harrick Scientific Corporation. The channel is machined in a $38 \times 38 \times 10$ mm block of stainless steel, with the flat side of a 25-mm-long, 23-mm-dia. hemicylindrical optical crystal forming one face. The flow inlet and outlet are provided through drilled 1/8-in. (3.2-mm) holes, with 1/8-in. (3.2-mm) tubing welded to the outside of the block above the holes. The flat side of the crystal is clamped nearly flush (a gap of less than 25 μm) to the metal plate using a Viton O-ring. Half the curved surface of the crystal was coated with silver to send the reflected infrared beam back to the crystal-fluid interface, thus doubling the signal. The incident angle of the infrared beam can be adjusted by rotating the entire flow assembly. Three ZnSe optical crystals, provided by Harrick, were used. (ZnSe is a standard material for ATR crystals because of its low absorption of light in the infrared region.) Thin metal coatings were deposited on the flat surfaces of two crystals, in one case approximately 15 to 20 nm of chromium, in the other approximately 10 nm of copper; these choices were based on components of the dies used in Ramamurthy's (1986) experiments. All surfaces were allowed to oxidize at ambient conditions.

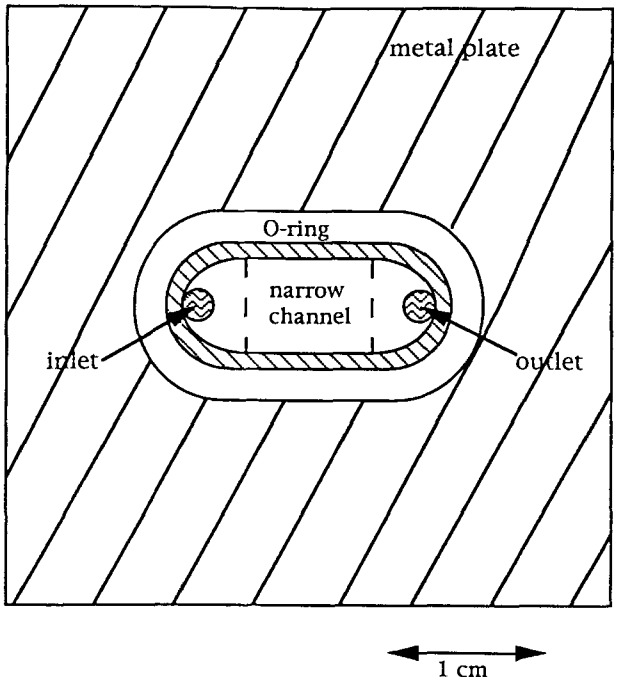

Figure 1. Top view of flow cell.

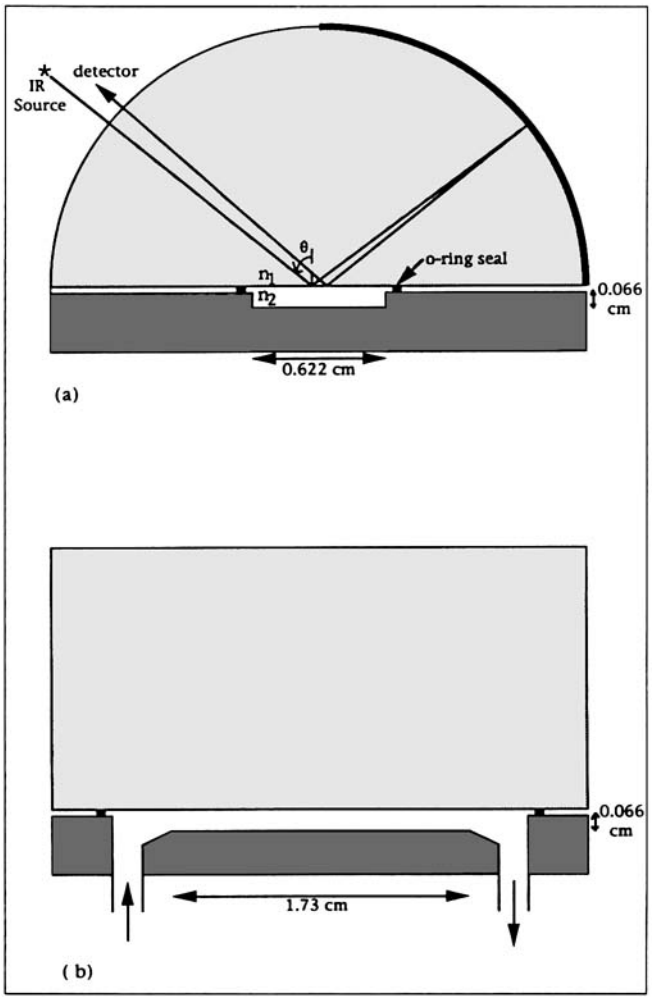

Figure 2. Schematic of the ATR flow cell.

(a) End view; (b) side view.

Two liquids were typically used sequentially in the flow system, the first denoted "tag" and the second "chase." The flow system is shown in Figure 3. One-eighth-in.-dia. (3.2-mm-dia.) stainless-steel tubing with Swagelock fittings was used throughout for the flow lines. Liquids could be injected by syringe (the tag) or pumped through continuously (the chase); in the latter case a variable speed gear pump (Micropump, model 185-000) with a stainless-steel housing, graphite gears, and Teflon seal was used. A Teflon filter was put in-line before the pump to remove particulates. Flow rates from 0.3 to more than 50 mL/min were achieved.

Two different valving systems were used to switch between the two fluids. Both systems allowed the pumped liquid to circulate and bypass the cell. Early experiments used one four-way and two three-way hand-actuated valves, as shown in Figure 3. The three-way valves were turned at the same time to switch the cell inlet and outlet connections from the syringe ports to the pumped-fluid lines. These valves were located within the FTIR sample compartment to minimize the liquid holdup and the volume of tubing to be swept by the pumped liquid. This arrangement required that the FTIR sample chamber be opened to switch the valves and then repurged before taking any IR spectra. Later experiments used an air-actuated eight-port, two-position valve (Figure 4) in which air actuation was effected from outside the sample chamber. In both cases an additional three-way valve was used to allow liquid to be pumped back to the feed vessel so that flow and temperature equilibrium could be established while bypassing the cell.

For experiments at temperatures above ambient the feed vessel was heated with a heating mantle, and the tubing upstream of the pump and between the rotameter and the sample chamber was wrapped with heating tape. The flow cell temperature was maintained with cartridge heaters inserted into the block and coated with magnesium hydroxide to enhance heat transfer. The temperature of the liquid in the cell was controlled with a thermocouple placed in the block and monitored with a thermocouple in the exit tubing.

Attenuated Total Reflection

When the refractive index n_1 of the optical crystal is greater than that of the sample, n_2, and light is projected onto the

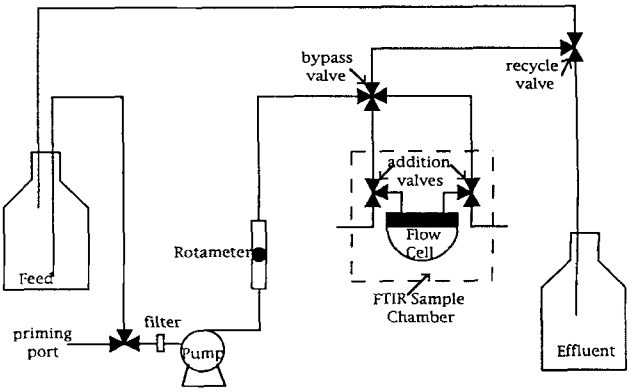

Figure 3. Schematic of the flow system.

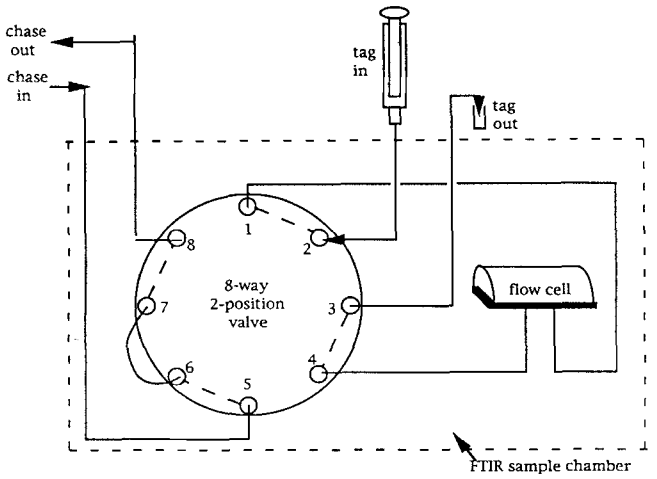

Figure 4. Schematic of the valving system.

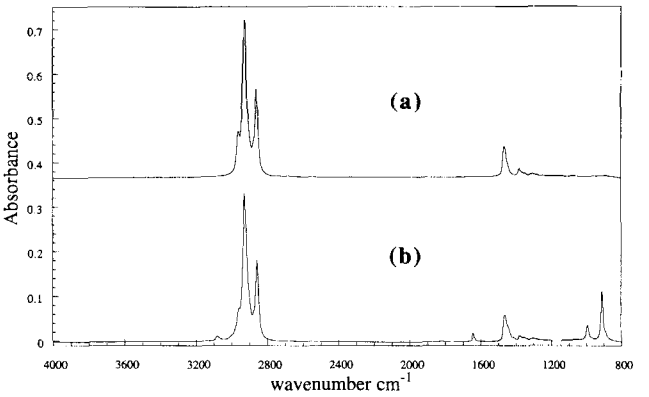

Figure 5. ATR/FTIR spectra.
(a)hexadecane; (b) 1-hexadecene.

optical crystal at an angle measured from the normal to the surface which is greater than a critical angle approximately equal to $\theta_c = \sin^{-1}(n_2/n_1)$, there is no transmitted beam into the sample; light is totally reflected at the interface, except for that which is absorbed by the sample. At the point of reflection, an evanescent (or nonpropagating exponentially-decaying) wave is formed in the sample medium. The energy in this wave is available to excite chemical bonds, and the absorbed energy can be detected. ATR theory is described by Hansen (1973), and approximate equations for weakly absorbing systems presented by Harrick (1967) are frequently used. ATR measurements probe the region near the surface; the penetration depth, defined as the distance into the sample medium where the electric field amplitude has fallen to $1/e$ of the value at the surface, is of the order of one wavelength for a weakly absorbing system. For ZnSe ($n_1 = 2.42$) and 1-hexadecene ($n_2 = 1.44$), with an incident angle of 55.9°, penetration depths range from 0.4 μm at 2,925 cm^{-1} to 1.26 μm at 910 cm^{-1}.

When a thin metal layer is placed between the optical crystal and a semiinfinite sample, the strongly absorbing nature of the metal will have an effect on the measured reflectance. The approximate equations of Harrick do not apply in general to this strongly absorbing system, and the exact equations of a three-medium system (or four-medium if an oxide layer is present) would be required. The components of the complex refractive index of very thin metal films (less than 20 to 30 nm) are wavelength- and thickness-dependent, and we lack adequate data for direct comparisons with theory. Quantitative comparisons between spectra taken under comparable conditions are still informative, however.

Fluids

Hexadecane, the longest alkane chain that is a liquid at room temperature, and 1-hexadecene, were chosen to model polyethylene. Both liquids were purchased from Aldrich Chemical Company and used as received. The hexadecane purity was listed as 99% and the 1-hexadecene as 93%, with less than 2.0% of 2-ethyl-1-tetradecene, 2-butyl-1-dodecene, 2-hexyl-1-decene, and *n*-hexadecane. Deuterated hexadecane was obtained from MSD Isotopes as 98.7 atom % deuterated, and was used as received. The deuterated hexadecane was used in some experiments in a 9.75 wt. % mixture with the hydrogenated hexadecane to obtain a fluid having the same density as 1-hexadecene.

Spectra

All spectra were taken on a Mattson Polaris FTIR spectrometer with a water-cooled Globar source emitting light in the midinfrared region (400 to 4,000 cm^{-1}). We used a narrow-range liquid-nitrogen-cooled mercury–cadmium–telluride detector with an effective long-wavelength cutoff around 750 cm^{-1}. An acceptable signal-to-noise ratio in the transient experiments required a compromise between spectral and temporal resolution. For slower flow rates we typically averaged over fifty scans at a resolution of eight wavenumbers. At faster flow rates we decreased the resolution to sixteen wavenumbers and averaged only twenty-five scans. We used software developed by Mattson to take continuous spectra.

Spectra of hexadecane and 1-hexadecene are shown in Figure 5. The C-H stretch bands near 2,925 cm^{-1} and the C-H bending bonds near 1,460 cm^{-1} are readily observed in both spectra. There are C-D bands in the hydrogenated/deuterated hexadecane mixture near 2,200 and 1,100 cm^{-1}. The major peak associated with the double bond of the 1-hexadecene occurs at 910 cm^{-1}. Exchange dynamics were determined by following the peak height at 910 cm^{-1} to determine the amount of 1-hexadecene present after spectral subtraction to remove hexadecane bands from the hexadecane–hexadecene mixture. The amount of hexadecane could also be determined by taking the difference between the height of the 2,925 cm^{-1} peak of the unsubstracted spectrum and the height of the same peak in the subtracted spectrum. The C-D peak at 2,200 cm^{-1} could be followed initially, but it disappeared into the noise before completion of an experiment. A net absorbance from a specified baseline was used with endpoints chosen to be within the noise level of zero absorbance areas on either side of the peak. The same baselines were used throughout any single experiment. Details of the data analysis are given in Dietsche (1993).

Experiments

The cell was flushed before each run with Freon-113 through the "tag" inlet and exit lines. (This solvent was chosen because the hydrocarbons are soluble in it, the vapor pressure is high enough to allow it to be removed by an air purge, it does not swell the O-ring seal, and it has readily identified infrared bands that could indicate the presence of residual solvent.) The cell was then dismantled and the O-ring soaked in Freon-113 for 30 to 60 min before being air-dried. The crystal was placed in an MEK bath for 30 to 60 min, then gently rubbed with an MEK-soaked cotton swab before being rinsed in succession with a 0.1-N HCl solution, distilled deionized water, and MEK. It was then placed under a filtered and dried air stream to dry. (The metal-coated crystals were not exposed to the acid solution.) The flow cell block was similarly cleaned. After the cell was reassembled and reconnected to the flow system, an air stream purge was connected to the cell overnight through the tag inlet and exit tubing.

A background single-beam spectrum of the empty cell was required first, using the same resolution and number of scans as the sample spectra. The tag species, which was preheated for high temperature runs, was introduced into the cell by syringe through the tag inlet port. When the valve arrangement in Figure 3 was used, the two three-way valves were switched to the flowthrough position and the sample compartment was allowed to purge again. At this point a spectrum of pure tag was taken.

To start a transient experiment, the flow rate of the chase fluid was set to the desired level (0.3 to 10 mL/min, corresponding to average linear velocities of 0.073 to 2.44 mm/min and apparent wall shear rates of 0.01 to 0.37 s^{-1}), with the four-way or eight-way valve set so that the fluid bypassed the cell. For high temperature runs, the heater circuits were turned on to bring the fluid up to the desired operating temperature. At a given time, the bypass valve was switched so that liquid was pumped through the cell. The change in concentration of species at the ATR crystal surface was monitored by following the change in the appropriate absorption bands.

When there was no longer any observable change in the spectra, or after a predetermined amount of time, the flow rate was increased to 50 mL/min for one or two minutes to flush any remaining tag from the cell and to obtain spectra of the pure chase liquid. In high temperature runs, the flow was reestablished at the lower flow rate and the temperature allowed to reequilibrate before obtaining the pure chase liquid spectra. Finally, the bypass valve was reswitched to stop the flow.

The exchange dynamics were studied by plotting the peak heights associated with the tag and chase species against time. The peak height axis can be normalized with respect to the peak height for the pure species to remove any differences in absolute absorbances between experiments. The absolute absorbance values were strongly affected by the crystal surface used, the incident beam polarization, and the temperature.

Results

A typical transient response is shown in Figure 6, where the normalized absorbance of 1-hexadecene with the ZnSe surface is plotted vs. time on semilogarithmic coordinates as it is displaced at room temperature by hexadecane. The broken line is a finite-element simulation of relative interfacial concentration using POLYFLOW (Crochet, 1992), assuming flow and diffusion but no surface interaction; diffusivities were estimated to be 3.1×10^{-6} cm^2/s. All experiments showed the same general features. There is an initial transient, well-represented by the simulation, which reflects bulk flow and diffusion from the wall region into the bulk. This is followed by a transition to a slow process that appears to be roughly first-order, with a characteristic time of order one minute; this appears to be a surface phenomenon. Error bars represent 90% confidence limits. Data during the final stage are not sufficiently precise to state with certainty whether or not the decay continues indefinitely or if there is a residual surface concentration of tag species. We found little difference in the use of hexadecene or hexadecane as the tag. A detailed discussion of the experiments, including differences between the responses of the two species which are too small to be relevant here, is given in Dietsche (1993).

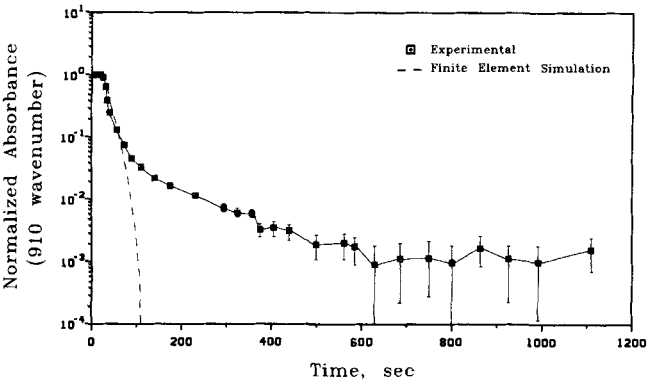

Figure 6. Normalized absorbance of 1-hexadecene as it is displaced by hexadecane at a flow rate of 1 mL/min, ZnSe crystal.

Error bars represent 90% confidence limits. The broken line is a finite-element simulation.

The apparent first-order process is highly dependent on both flow rate and surface composition. Room-temperature data in the first-order region for the copper-coated surface are shown in Figure 7. It is notable that all data extrapolate

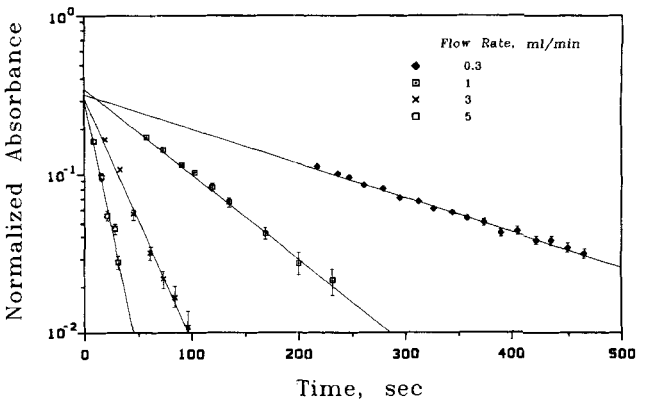

Figure 7. Normalized absorbance of hexadecane displaced by 1-hexadecene for different flow rates, copper-coated crystal.

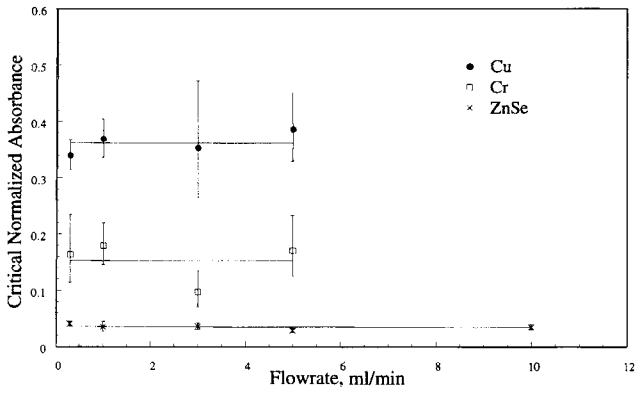

Figure 8. Intercepts of the first-order region as functions of flow rate for the three crystal surfaces, 1-hexadecene displaced by hexadecane.

to roughly the same intercept at $t = 0$. The intercept may be interpreted as reflecting a critical near-surface concentration at which the surface interactions of the chains dominate the flow and diffusion process. The intercepts are shown as functions of flow rate for all three crystals in Figure 8. In all cases they are relatively independent of flow rate, but strongly dependent on the nature of the surface. The critical concentration decreases in the order Cu > Cr > ZnSe.

The apparent first-order time constant at room temperature is plotted in Figure 9 as a function of flow rate for each surface. There is a strong dependence on flow rate. Decay at each flow rate is fastest for Cu, followed by Cr and ZnSe. (The 90% confidence limits overlap at 0.3 mL/min.)

Experiments were also carried out at 60 and 90°C at two flow rates, 0.3 and 5 mL/min, and activation energies were estimated from a plot of the logarithm of the time constant vs. reciprocal temperature. The values, shown in Table 1 with standard errors, are of the order that would be expected for physisorption, as would be expected for the simple hydrocarbons studied here. It is interesting to note that the estimated activation energy for the ZnSe surface increases with flow rate, while those for the metal surfaces decrease.

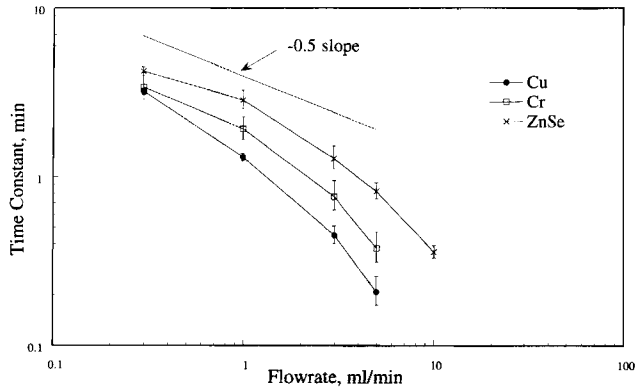

Figure 9. Time constants for the first-order region as functions of flow rate for the three crystal surfaces, 1-hexadecene displaced by hexadecane.

Table 1. Activation Energies

	Flow Rate (mL/min)	Activation Energy (kcal/mol)
ZnSe	0.3	0.33 ± 0.17
	5	3.00 ± 0.93
Cr	0.3	2.13 ± 0.26
	5	1.39 ± 0.12
Cu	0.3	4.84 ± 0.04
	5	1.80 ± 1.33

Surface Features

All three crystal surfaces were examined after completion of the flow experiments with optical microscopy and scanning electron microscopy (SEM). SEM images are shown in Figure 10. There were a few small spots on the metal-coated crystals, approximately 0.1 to 1 μm across, where the metal coating was gone; the chrome-coated crystal had a few larger spots of order 25 to 75 μm. Most of the metal had been stripped off near the O-ring seal and at the edges of the crystal surface. There were thin straight scratches on all crystals of order 0.05 to 0.3 μm in width, and small pits of order 0.1 to 0.2 μm across. The direction of the scratches seemed to be random on the ZnSe and chrome-coated crystals, but the scratches were aligned almost orthogonal to the flow direction on the copper-coated crystal. The scratches on the metal surfaces did not seem to penetrate to the crystal. The density of scratches on the ZnSe surface was lower than on the metal surface, but there were also some larger (0.5 μm across), long (4 to 14 μm) jagged defects present. Light, colorful spots on the order of 10 μm in diameter were present on all three crystals; these might be crystal defects or gouges, and the metal coatings appeared to cover the spots.

We examined the areas near the centers of the crystal faces with an optical profilometer. Root-mean-square (RMS) and maximum peak-to-valley (P–V) values for the vertical roughness are recorded in Table 2. The topographies are not significantly different for the three surfaces, and the roughness is probably indicative of the scratches and pits seen with microscopy. The similarity of the profiles suggests that they reflect the topography of the underlying ZnSe substrate.

Discussion

The long time constants for species exchange suggest the presence of a surprisingly strong interaction between the oligomeric polyolefins and the solid surfaces. The presence of a surface effect is emphasized by the data in Figure 9, where the time constant may be considered to be equivalent to the reciprocal of an overall mass-transfer coefficient. Ruckenstein (1987) has used scaling arguments to demon-

Table 2. Surface Roughness from Optical Profilometry

	RMS (nm)	*P-V* (nm)
ZnSe	6.1	165
Chrome	5.7	138
Copper	6.0	123

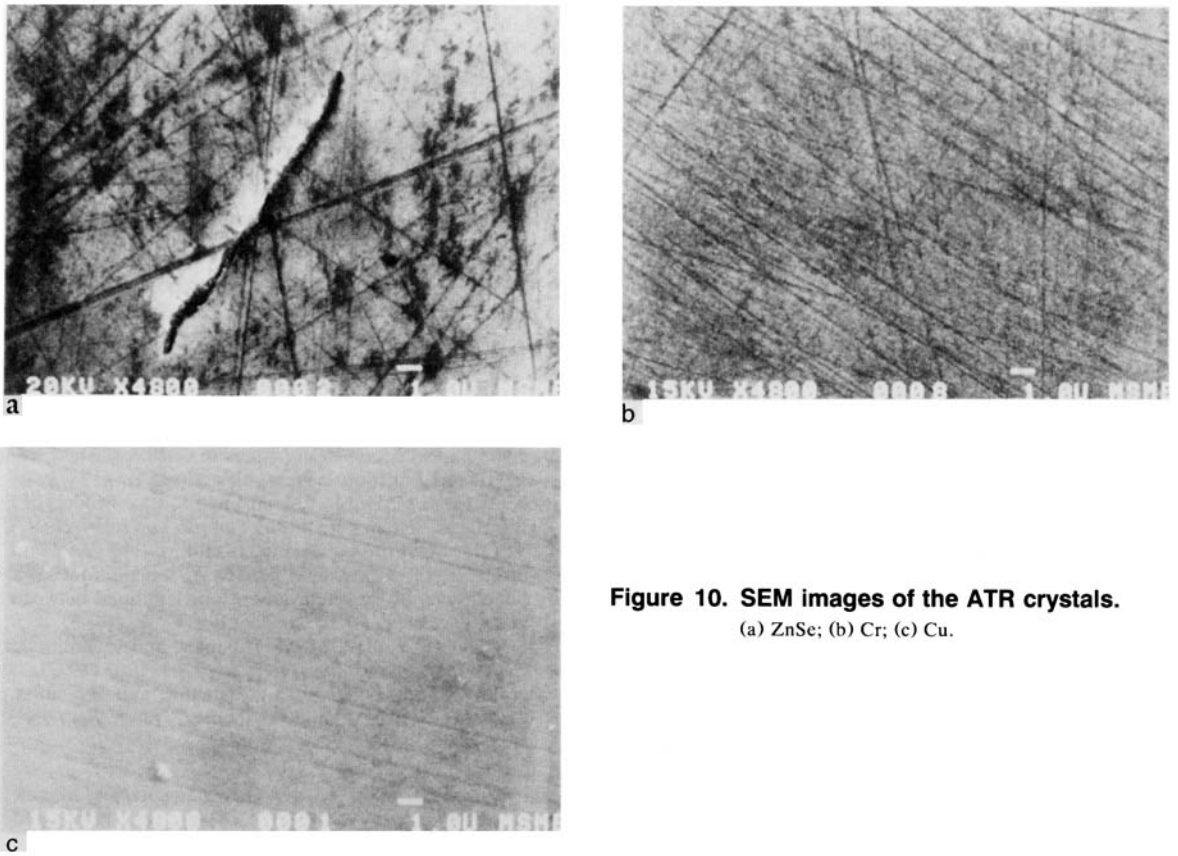

Figure 10. SEM images of the ATR crystals.
(a) ZnSe; (b) Cr; (c) Cu.

strate that a power-law dependence of the Sherwood number on the Reynolds number cannot have an exponent greater than 0.5 for laminar flow with diffusion. A line with slope -0.5 is drawn in Figure 9, and it is clear that the magnitude of an equivalent power-law exponent is significantly greater than 0.5 at the higher flow rates. Hence, an additional physical mechanism, which we believe to be associated with adsorption, must be relevant.

The picture that seems to emerge is an entropically driven flow-rate- (or stress-) dependent adsorption equilibrium that retards the exchange between the surface and bulk. The weakest adsorption would correspond to a high critical wall concentration ("floppy" chains with a small number of surface contact points) and rapid depletion, while the strongest adsorption would correspond to a small critical wall concentration (tightly bound chains) and slow depletion and replacement. We expect the strength of adsorption of hexadecane to be in the order Cr > Cu (Burkstrand, 1981), which is consistent with this model.

There is one possible inconsistency. The model of Scheutjens and Fleer for competitive surface interactions of long-chain molecules at steady state (Scheutjens, 1992), applied to the adsorption of sixteen-monomer-unit molecules with similar adsorption energies per monomer, predicts that the more strongly adsorbing molecule has a slightly higher fraction of monomer units in trains along the surface, but the bulk value of concentration is reached within five monomer units from the surface (J. M. H. M. Scheutjens, personal communication, 1991). This corresponds to a surface layer of about 1 nm for hexadecane. For the ZnSe surface we can use the approximate ATR equations of Harrick to estimate a film thickness of about 6.5 nm, which seems excessive. The rough surface topography, with an RMS variation of 6 nm and pits and grooves, may provide the resolution, since there is excess surface area and locations where many monolayers could remain.

The situation studied here has not been analyzed theoretically, but there are some molecular dynamics calculations of *n*-alkanes near surfaces under more constrained conditions that may be relevant (Bitsanis and Pan, 1993; Pan and Bitsanis, 1993; Winkler et al., 1993; Xia et al., 1992; Xia and Landman, 1993). It is found that *n*-alkanes favor a stretched conformation at the surface, with molecular ordering and densification relative to the bulk. This causes a reduction in mobility orthogonal to the surface and consequently slower dynamics. Such a mechanism could be the cause of the sluggish dynamics for chain exchange observed in the present work. It is significant that we do not see the stretched exponential behavior suggested by Douglas et al. (1993) as characteristic of the regime of slow desorption at polymer interfaces.

Conclusions

The ATR/FTIR experiments reveal a surprising interaction between the weakly adsorbing oligomeric polyolefins and

the surface, which manifests itself in slow exchange between the surface and the bulk. Interactions of this type are likely to have an impact in the wall region for polymer flow, since segmental motions of chains near the surface will be greatly retarded. The relevance to apparent wall slip and instabilities is unclear, since extrapolation of oligomeric results to entangled chains is not always possible.

Acknowledgment

This work was supported by the Director, Office of Energy Research, Office of Basic Energy Sciences, Materials Science Division of the U.S. Department of Energy under Contract No. DE-/AC03-76SF00098. Laura Dietsche received fellowship support from the National Science Foundation, the University of California, and the IBM Corporation.

Literature Cited

Bitsanis, I. A., and C. M. Pan, "The Origin of Glassy Dynamics at Solid Oligomer Interfaces," *J. Chem. Phys.*, **99**, 5520 (1993).

Burkstrand, J. M., "Metal-Polymer Interfaces: Adhesion and X-Ray Photoemission Studies," *J. Appl. Phys.*, **52**, 4795 (1981).

Crochet, M. J., *Applications of Computer Modeling for Extrusion and Other Continuous Polymer Processes*, K. T. O'Brien, ed., Hanser, Munich (1992).

Denn, M. M., "Surface-Induced Effects in Polymer Melt Flow," *Theoretical and Applied Rheology*, P. Moldenaers and R. Keunings, eds., Elsevier, Amsterdam, p. 45 (1992).

Dietsche, L. J. R., "Surface Interactions in a Shear Field," PhD Diss., Univ. of California, Berkeley (1993).

Douglas, J. F., H. E. Johnson, and S. Granick, "A Simple Kinetic Model of Polymer Adsorption and Desorption," *Science*, **262**, 2010 (1993).

Granick, S., "Dynamics of Adsorption and Desorption at Polymer/Solid Interfaces," *Physics of Polymer Surfaces and Interfaces*, I. C. Sanchez, ed., Butterworth-Heinemann, Boston, p. 227 (1992).

Hansen, W. H., "Internal Reflection Spectroscopy in Electrochemistry and Electrochemical Engineering," *Advances in Electrochemistry and Electrochemical Engineering*, R. H. Muller, ed., Wiley, New York (1973).

Harrick, N. J., *Internal Reflection Spectroscopy*, Harrick Scientific Corp., Ossining, NY (1967).

Johnson, H. E., S. J. Clarson, and S. Granick, "Overshoots as Polymers Adsorb," *Polymer*, **34**, 1960 (1993).

Pan, C. M., and I. Bitsanis, "Structure, Conformation and Dynamics of Polymer Chains at Solid Melt Interfaces," *Makromol. Chem., Macromol. Symp.*, **65**, 211 (1993).

Ramamurthy, A. V., "Wall Slip in Viscous Fluids and Influence of Materials of Construction," *J. Rheol.*, **30**, 337 (1986).

Ruckenstein, E., "Analysis of Transport Phenomena Using Scaling and Physical Models," *Advances in Chemical Engineering*, Vol. 13, J. Wei, ed., Academic Press, Orlando, p. 11 (1987).

Scheutjens, J. M. H. M., "Mean-Field Lattice Models of Polymers at Interfaces," *Physics of Polymer Surfaces and Interfaces*, I. C. Sanchez, ed., Butterworth-Heinemann, Boston, p. 117 (1992).

Winkler, R. G., T. Matsuda, and D. Y. Yoon, "Stochastic Dynamics Simulations of Polymethylene Melts Confined between Solid Surfaces," *J. Chem. Phys.*, **98**, 729 (1993).

Xia, T. K., O. Y. Jian, M. W. Ribarsky, and U. Landman, "Interfacial Alkane Films," *Phys. Rev. Lett.*, **69**, 1967 (1992).

Xia, T. K., and U. Landman, "Structure and Dynamics of Surface Crystallization of Liquid *n*-Alkanes," *Phys. Rev. B—Condensed Matter*, **48**, 11313 (1993).

Manuscript received Apr. 6, 1994, and revision received Aug. 23, 1994.